OATAO

Open Archive Toulouse Archive Ouverte

Open Archive Toulouse Archive Ouverte (OATAO)

OATAO is an open access repository that collects the work of some Toulouse researchers and makes it freely available over the web where possible.

This is an author's version published in: https://oatao.univ-toulouse.fr/27082

Official URL: https://doi.org/10.2514/6.2018-4215

To cite this version :

Any correspondence concerning this service should be sent to the repository administrator: tech-oatao@listes-diff.inp-toulouse.fr

Linear stability analysis in rotating frames and its application to fan blade transition prediction

L. Pascal[*]

ONERA/DMPE, Université de Toulouse - F-31055 Toulouse - France

R. Barrier[†], G. Billonet[‡], J. Marty[§]

ONERA/DAAA, Université Paris-Saclay - F-92190 Meudon - France

The in-house linear stability solver of ONERA has been extended to rotating frames. The theoretical details of linear stability theory in rotating frames are given. Validation is performed by comparing against the well-known Ekman layer case. Moreover, two new compressible validation cases are proposed for which very good agreement is as well obtained. Linear stability analysis is then performed on a flow around a rotating fan blade, obtained by means of RANS computation. By neglecting or taking into account rotation in the linear stability equations, the effect of rotation on transition mechanisms is investigated. Moreover, N-factors are computed for transition prediction. The present results show that rotation hardly modifies the growth-rate of Tollmien-Schlichting instabilities. However, rotation destabilizes stationary cross-flow waves but not enough to trigger transition.

I. Nomenclature

α	=	Streamwise wave number
β	=	Transversal wave number
β_0	=	Angle between the wall friction vector and the velocity vector at the boundary layer edge
ω	=	Angular frequency
$\underline{\Omega}$	=	Rotation vector
ψ	=	Angle between boundary layer edge streamline and wave vector
s	=	Curvilinear abscissa
$\underline{x} = (x, y, z)$	=	Local stability frame
x	=	Coordinate oriented along the streamline at the boundary layer edge
y	=	Wall normal coordinate

II. Introduction

Natural transition prediction on wings and nacelles has received much attention over the past years as it has a significant impact on wall friction and heating. Linear stability analysis has been extensively used to study boundary layer instabilities at the origin of laminar to turbulent transition, namely Tollmien-Schlichting and cross-flow waves. The e^N method [1] and all its derivatives, that are based on linear stability theory, are commonly used for transition prediction on wings and nacelles for instance.

As far as flows around rotating geometries are concerned (wind turbines, helicopter and fan blades, etc . . .), laminar to turbulent transition has been experimentally studied for decades, see for instance the work of Mc Croskey [2] (for helicopter blades) or the quite recent papers of Schülein et al. [3] and Lang et al. [4]. While linear stability theory has been applied for simple geometry in rotating frame: disks [5], cones [6] and flat plates [7], little is known about the impact of rotation on transition mechanisms on rotating blades. In reference [4], e^N is used to predict transition on a rotor blade and Gross et al. [8] performed stability analysis of the flow over a wind turbine blade. But in both studies,

---

[*]Research Scientist, Multi-Physics and Energetics Department, lucas.pascal@onera.fr
[†]Research Scientist, Aerodynamic, Aeroelasticity and Acoustics Department
[‡]Research Scientist, Aerodynamic, Aeroelasticity and Acoustics Department
[§]Research Scientist, Aerodynamic, Aeroelasticity and Acoustics Department

the authors did not seem to account for the additional terms related to centrifugal and Coriolis accelerations in the linear stability equations.

This paper presents the details for extending the instability analysis program MAMOUT [10] of ONERA to rotating flow (section III). In particular, test cases are provided to validate the implementation of the additional terms appearing in the linear stability equations for compressible flows over arbitrary geometries because, as stated by Dechamps and Hein [11], "only very few test cases combine rotation with compressibility in the literature". The solver MAMOUT is then applied to investigate the effect of the terms associated to rotation in the linear stability equations on the stability of the flow over a fan blade (section IV).

III. Extension of a linear stability solver to flows over rotating geometries

A. Local linear stability equations

Linear stability equations (see for instance reference [12] for comprehensive details for incompressible flows) are obtained by considering the Navier-Stokes equations applied to a flow $Q(\underline{x}, t)$ (of velocity vector $\underline{U}$ and density ρ) divided into a steady mean-flow $Q_0(\underline{x})$ (of velocity vector $\underline{U}_0$ and density ρ_0) and an unsteady perturbation term $q'(\underline{x}, t)$ (of velocity vector $\underline{u}'$ and density ρ'). If the latter is assumed to be of small magnitude, nonlinear terms are neglected and linearized Navier-Stokes equations, governing the evolution of q', are obtained. Under the parallel flow assumption, the equations are further simplified and the perturbation is written under the wave Ansatz $q'(\underline{x}, t) = \hat{q}(y) \exp(i(\alpha x + \beta z - \omega t))$. Spatial local linear stability analysis [1] consists finally in fixing β and ω and solving the resulting eigenproblem of eigenvalues α. The growth rate of a wave of streamwise wavenumber α is then given by $-\Im(\alpha)$.

In a rotating frame, two new terms appear in the Navier-Stokes equations: the Coriolis acceleration term $2\rho\underline{\Omega} \wedge \underline{U}$ and the centrifugal acceleration term $\rho\underline{\Omega} \wedge (\underline{\Omega} \wedge \underline{r}(M))$ where M is the current point and $\underline{r}(M)$ is the vector from the projection of the point M on the rotation axis to M. When following the linearization process described above, the linearized Navier-Stokes equations in a rotating frame are enhanced with[*]:

$$2\rho_0\underline{\Omega} \wedge \underline{u}' + 2\rho'\underline{\Omega} \wedge \underline{U}_0 + \rho'\underline{\Omega} \wedge (\underline{\Omega} \wedge \underline{r}(M)) . \tag{1}$$

B. Implementation and validation

The additional terms associated to rotation given in Eq. (1) have been added in the ONERA in-house linear stability solver MAMOUT.

The solver features the possibility to consider only one of three new additional terms. In the following three sections, the implementation of each term is validated independently. The second and third configurations are not physically relevant but are just constructed for the sake of validation of the implementation of the compressible terms.

1. First Coriolis acceleration term

The implementation of the term $2\rho_0\underline{\Omega} \wedge \underline{u}'$ is validated on the incompressible Ekman layer flow. This configuration has been extensively studied, see for instance Ref. [13]. In the latter reference are given eigenvalues. In particular the first line of Ref. [13, Table 1.] is considered and compared against results of MAMOUT in figure 1 (eigenvalues are plotted in terms of phase velocity $c_\phi = \omega/\alpha$). A very good agreement is obtained both for incompressible and compressible linear stability computations. Moreover, MAMOUT catches the continuous spectrum, see Ref. [14].

2. Second Coriolis acceleration term

In order to validate the term $2\rho'\underline{\Omega} \wedge \underline{U}_0$, a configuration has been made up. It consists of a channel uniform flow of Mach number $M_x = U_0/a_0$ and $M_z = W_0/a_0$ along x and z respectively. The upper and lower bounds of the channel are located at $y = H$ and $y = 0$ respectively. The viscosity is set here to zero and the governing equations of the perturbations are reduced to the standard linearized Euler equations enhanced by the term $2\rho'\underline{\Omega} \wedge \underline{U}_0$. For given values

---

[*]The energy equation remains unchanged.
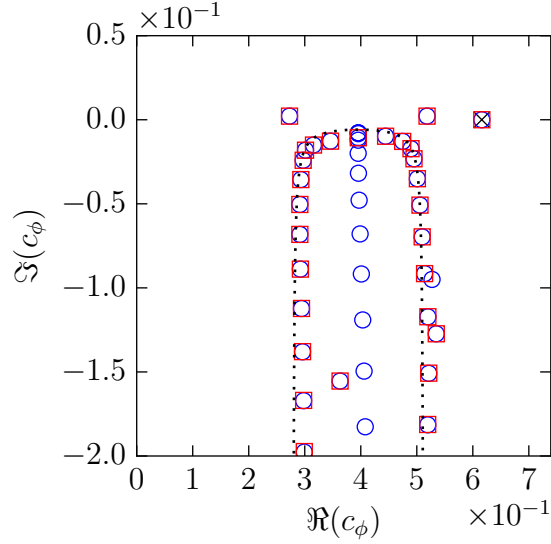
Fig. 1 **Incompressible (▢) and compressible (◯) spectra, eigenvalue given in Ref. [13] (×), continuous spectrum (Ref. [14]) (- - -).**

of ω and β, the wavenumber along x of the acoustic mode of order $|m| > 0$ along y is given by:

$$\alpha_m^{\pm} = \frac{M_x \dfrac{\omega}{a_0} - \beta M_x M_z - iM_z \dfrac{\Omega_y}{a_0} \mp \sqrt{\alpha_1 + \alpha_2 + \alpha_3 - \alpha_4 - \left(\dfrac{\Omega_y}{a_0}\right)^2 M_z}}{M_x^2 - 1}, \tag{2a}$$
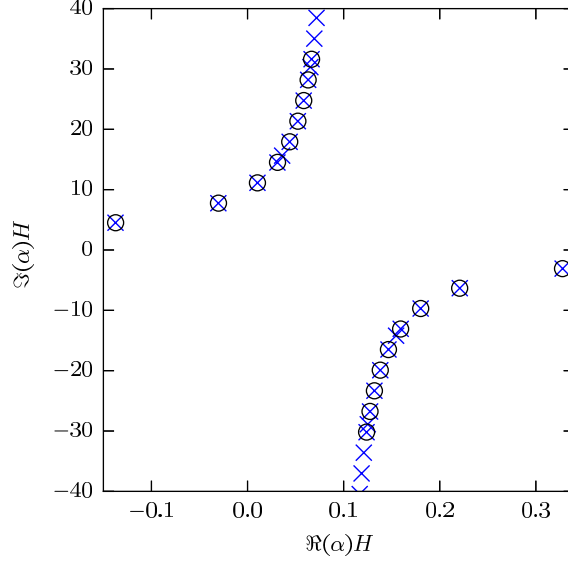
where

$$\alpha_1 = \left(\left(\frac{m\pi}{H}\right)^2 + \beta^2 + 2i\beta M_x \frac{\Omega_y}{a_0}\right)\left(M_x^2 - 1\right),$$

$$\alpha_2 = \left(\beta M_z - \frac{\omega}{a_0}\right)\left(\beta M_z - \frac{\omega}{a_0} + 2iM_x M_z \frac{\Omega_y}{a_0}\right),$$

$$\alpha_3 = \left(M_x^2 \frac{\Omega_z}{a_0} - M_x M_z \frac{\Omega_x}{a_0}\right)^2,$$

$$\alpha_4 = M_x \frac{\Omega_z}{a_0} - M_z \frac{\Omega_x}{a_0}.$$

On Fig. 2 are compared the wavenumbers obtained numerically and analytically for $M_x = 0.4$, $M_z = 0.3$, $\underline{\Omega}H/a0 = (1, 2, 3)$, $\beta = 1/H$ and $\omega = 0.1a_0/H$. A very good agreement is observed (the relative deviation is between 10^{-5} and 10^{-3} for $|m| \in [\![1, 10]\!]$).

3. Centrifugal acceleration term

As in the previous section, the configuration considered here is quite unrealistic but may be used to validate the implementation of the term $\rho' \underline{\Omega} \wedge (\underline{\Omega} \wedge \underline{r}(M))$. The same base flow is considered but here $\underline{\Omega} = \Omega e_y$ (therefore $\underline{r}(Q) \cdot e_y = 0$ and $\forall Q \; \underline{r}(Q) = \underline{r}(O)$). Solving analytically the linearized Euler equations enhanced by $\rho' \underline{\Omega} \wedge (\underline{\Omega} \wedge \underline{r}(M))$ for a given couple (ω, β) yields the following streamwise wavenumber:

$$\alpha_m^{\pm} = \frac{\dfrac{\omega}{a_0} M_x - \beta M_x M_z + \dfrac{i}{2}\underline{r}(O) \cdot \underline{e_x} \left(\dfrac{\Omega_y}{a_0}\right)^2 \mp \sqrt{\alpha_1 + \alpha_2 + \alpha_3 + \alpha_4 - \left(\dfrac{\underline{r}(O) \cdot \underline{e_x}}{2}\right)^2 \left(\dfrac{\Omega_y}{a_0}\right)^4}}{M_x^2 - 1} \tag{3a}$$

3

Fig. 2 Numerical spectrum (crosses) and analytic wavenumber given by eq. (2a) (circles) for $|m| \in [\![1, 10]\!]$.

$$\alpha_1 = \left(M_x^2 - 1\right) \left(\left(\frac{m\pi}{H}\right)^2 + \beta^2\right)$$

$$\alpha_2 = \left(\frac{\omega}{a_0} - \beta M_z\right)^2$$

$$\alpha_3 = \mathrm{i}\beta \, \underline{r}(O) \cdot \underline{e}_z \left(\frac{\Omega_y}{a_0}\right)^2 \left(M_x^2 - 1\right)$$

$$\alpha_4 = \mathrm{i} \, \underline{r}(O) \cdot \underline{e}_x \left(\frac{\Omega_y}{a_0}\right)^2 \left(\frac{\omega}{a_0} M_x - \beta M_x M_z\right)$$

The comparison between the analytical and numerical wavenumbers is displayed on Fig. 3. The parameters are $M_x = 0.4$, $M_z = 0.3$, $\underline{\Omega} = 2a_0/H\underline{e}_y$, $\underline{r}(Q) = 5H\underline{e}_x + 3H\underline{e}_z$, $\omega = 0.3a_0/H$ and $\beta = 1/H$. For $|m| \in [\![0, 10]\!]$, the relative deviation is at most 4.5×10^{-5}.

IV. Application to fan blade transition prediction

Stability of a boundary layer over a fan blade is analyzed in this section. The primary objective is to investigate how rotation might modify the transition mechanisms. As the latter are strongly related to linear instabilities, this is achieved by comparing linear stability results obtained by neglecting the rotation terms (eq. (1)) with linear stability computations accounting for the rotation terms.

A. Flow computation

The mean-flow on which linear stability analysis is performed corresponds to the laminar region of a RANS field obtained with the elsA software (ONERA-Airbus-Safran property). elsA computation was run with second order Roe's spatial scheme. Transition was accounted for by means of ONERA transition criteria (AHD-Gleyzes, C1) and Roberts criterion (with $Tu = 0.5\%$), see Ref. [16] for more details.

The mesh is built to be orthogonal to the blade in the boundary layer. There are about 50 cells in the boundary layer thickness in the laminar region and a moderated ratio is chosen for the geometric progression. Such parameters are known to be reasonable good for transition prediction in elsA . They correspond to minimal requirements for exact stability analysis.

4
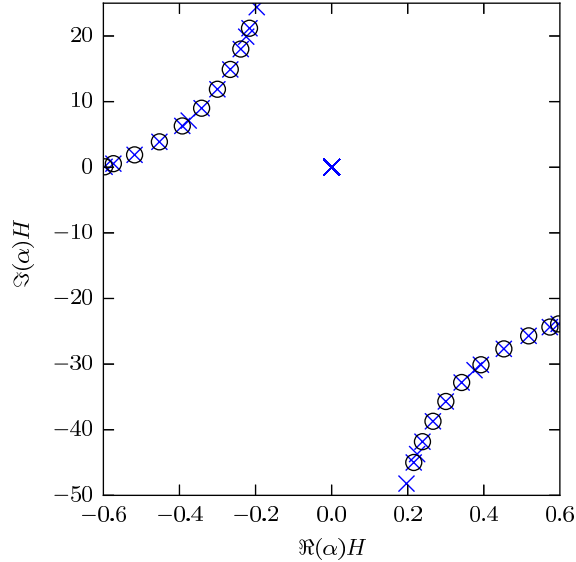
Fig. 3 **Numerical spectrum (crosses) and analytic wavenumber given by eq.** (3a) **(circles) for** $|m| \in [\![0, 10]\!]$.

Post-processing of the elsA computation shows that transition is only triggered by AHD-Gleyzes criterion i.e. according to elsA transversal transition mechanisms associated to stationary cross-flow waves (modeled in elsA by C1 criterion) do not trigger transition: transition is due to longitudinal mechanisms only.

B. Flow topology

In order to highlight regions subject to boundary layer separation on both sides, friction lines are plotted in figures 4(a,c) together with regions where $|\beta_0| > \pi/2$ (which corresponds to flow separation). Transition location (i.e. where the intermittency starts to grow) is plotted as a thick pink line. At the suction side, leading edge separation occurs from the hub up to approximately mid span and near the tip. This separation triggers laminar to turbulent transition. From about 50% to 75% of the blade span, the flow exhibits a laminar zone. A quite significant laminar zone is observed at the pressure side.

Streamlines at the boundary layer edge at the suction side (respectively pressure) are plotted in figure 4(b) (respectively figure 4(d)). There are basically oriented along the chord like the friction lines, which shows that the cross-flow is weak (which is consistent with the fact that C1 criterion does not trigger transition).

C. Linear stability analysis

1. Analysis at a given location

Before integrating the growth rate $(-\Im(\alpha))$ to get N-factors, stability analysis is performed at three locations P1, P2 and S1 (depicted with black squares on figures 4(a,c)). At each location, linear stability computations are run over a wide range of transverse wavenumbers β and angular frequencies ω. By running two sets of computations, one where rotation terms are accounted for and one where they are neglected, the effect of rotation on linear instabilities is investigated. The computed contours of $\Im(\alpha)$ are plotted figures 5(a-f). From a qualitative point of view, the rotation does not seem to affect much the value of the growth rate.

In order to have a more quantitative point of view, $\Im(\alpha)$ is plotted in figures 6(a-f) as a function of ψ for $\omega = 0$ and for the value of the angular frequency that leads to the highest growth rate when rotation is not accounted for. The conclusions are quite the same at the three locations. The range of ψ and the value of $\tilde{\omega}$ are characteristics of stationary cross-flow (figures 6(a,c,e)) and Tollmien-Schlichting (figures 6(b,d,f)) instabilities. Stationary cross-flow waves are destabilized by rotation but the growth rate achieved is one order of magnitude lower than the growth rate of Tollmien-Schlichting waves. The latter are hardly affected by the rotation.
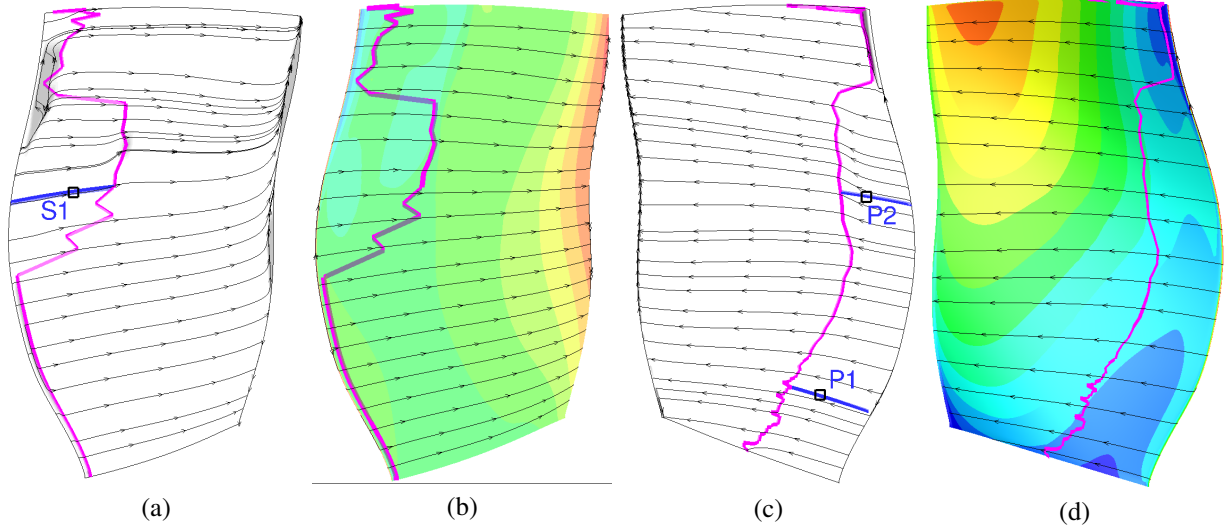
Fig. 4 (a) and (c): Friction lines at suction (a) and pressure (c) sides. The grey regions show where $|\beta_0| > \pi/2$. (b) and (c): streamlines at suction (b) and pressure (d) sides and pressure contours. On all four figures, the thick pink line shows predicted transition locations in elsA.

Rotation has not been found to generate new types of instabilities, contrary to what Dechamps and Hein [11] obtained for a flat plate flow. The latter authors observed "the appearance of a new region of instability at smaller α_r [here $\Re(\alpha)$] and higher β". Such wavenumbers are characteristics of cross-flow instabilities. Contrary to the configuration studied by Dechamps and Hein [11], the flow over a fan blade supports cross-flow waves even when rotation is not accounted for. Adding the rotation terms in the linear stability equations is only seen to destabilize the already existing cross-flow waves. The fact that Tollmien-Schlichting instabilities are hardly modified is in agreement with results of Dechamps and Hein [11].

2. Computation of N-factors

In order to evaluate a more global effect and to draw some conclusion on transition prediction, N-factors are computed along the lines P1, P2 and S1 (depicted by blue lines in figures 4(a,c)). A first attempt has been made to interpolate the field along streamlines but it yielded non-smooth boundary layer profiles. Therefore it has been chosen to approximate the streamlines by taking closest cells centers which actually corresponds to taking mesh lines. Since both the flow and the mesh lines are oriented along the chord, taking the mesh lines seems to be a justified approximation.

The computation is performed following the envelope method [1]:

$$N = \max_{\omega} \int_{s < s_{\gamma > 0}} \max_{\beta} -\Im(\alpha) \mathrm{d}s. \tag{4}$$

s is the curvilinear abscissa along the considered line and the range of integration is restricted to the laminar regions of the mean-flow field (corresponding to $s < s_{\gamma > 0}$). Please note that when transition is detected in elsA, the intermittency does not start immediately to grow for the sake of numerical stability. The locations where transition is detected in elsA along lines P1, P2 and S1 are plotted as vertical dotted lines on figures 7(a), 8(a) and 9(a).

N-factors for Tollmien-Schlichting and cross-flow waves along line P1 are plotted on figure 7. As observed in section IV.C.1, accounting for rotation does not affect significantly Tollmien-Schlichting instabilities. However rotation destabilizes cross-flow waves but the value of N achieved is too low to trigger transition. Similar trends are observed along lines P2 and S1, see figures 8 and 9.

Transition locations correspond to locations where the envelope of Tollmien-Schlichting instabilities reaches the threshold value given by the Mack's law (plotted as horizontal dotted lines in figures 7(a), 8(a) and 9(a):

$$N_T = -8.43 - 2.4 \ln(Tu = 0.5\%) = 4.3. \tag{5}$$

In terms of transition prediction, elsA and exact stability computations are in good agreement along line P2. However, elsA slightly underpredicts the transition location along line P1 while along line S1 the transition location is found
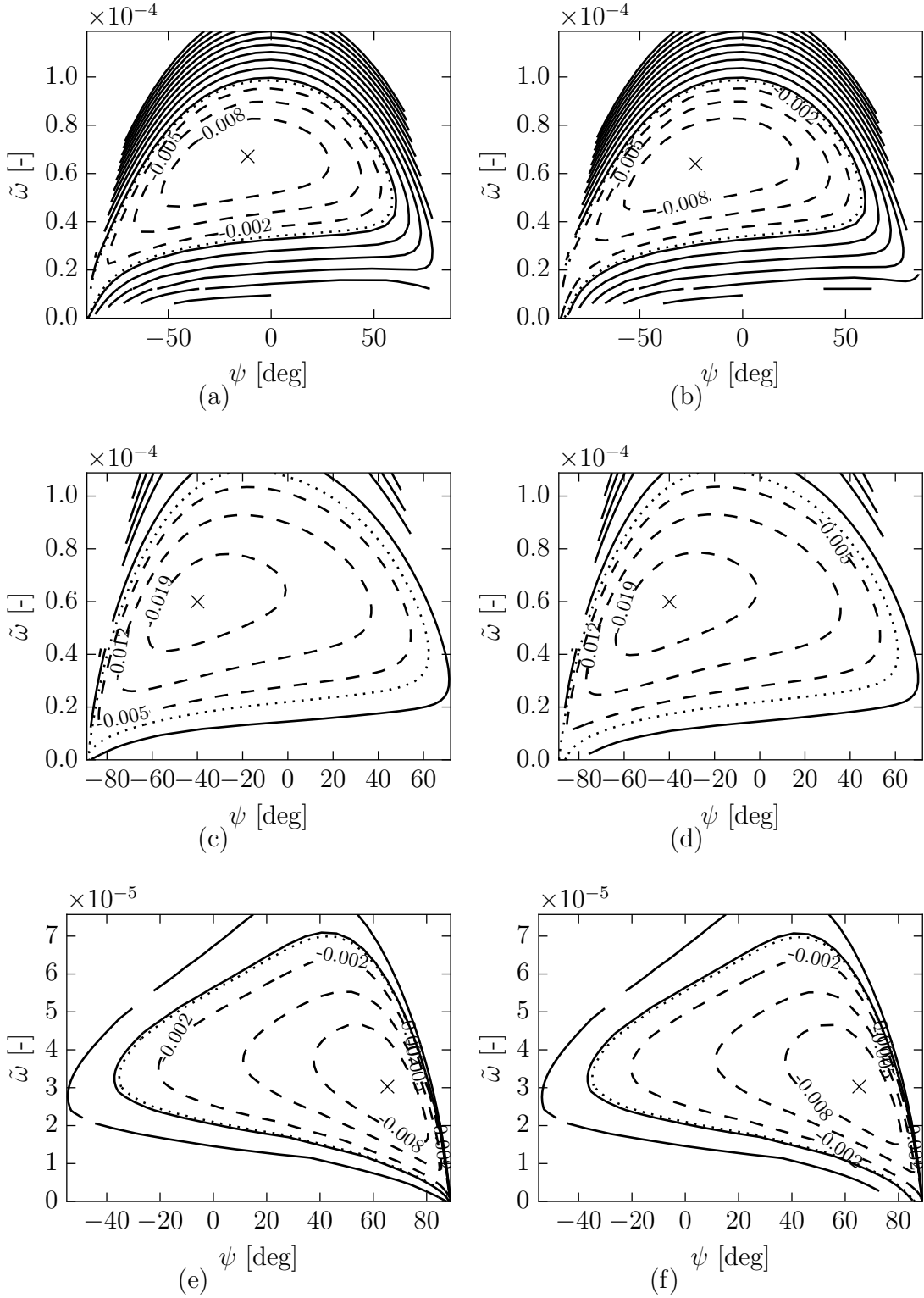
Fig. 5 Contours of $\Im(\alpha)\delta_1$ at locations P1 (a,b), P2 (c,d) and S1 (e,f). On the left plots, the rotations terms are not accounted for while they are taken into account on the right plots. The zero contour is dotted, solid and dashed lines depict positive and negative contours respectively. The cross symbol depicts the highest growth rate.
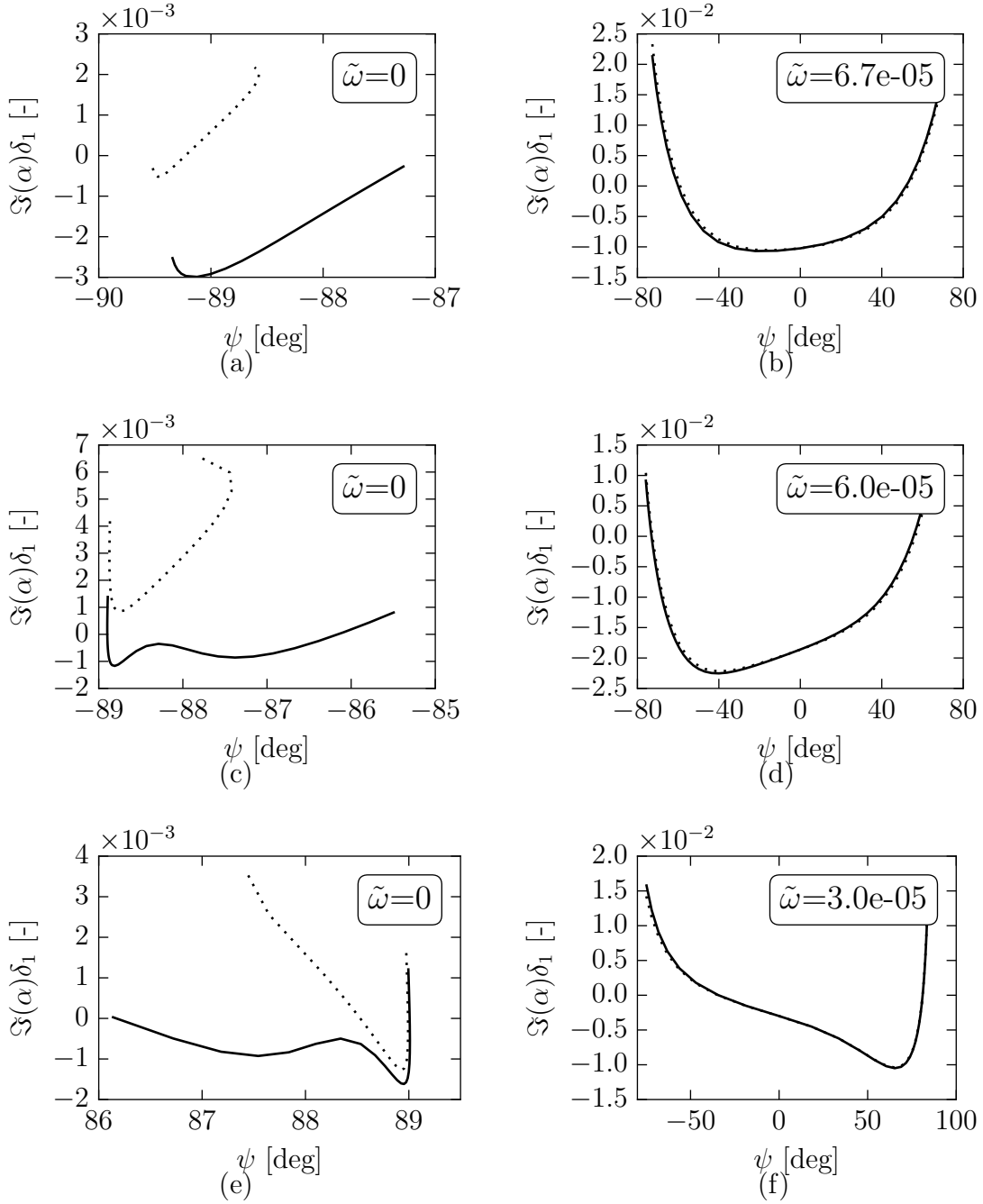
Fig. 6 Imaginary part of the axial wavenumber against ψ for a fixed value of the angular frequency (given in each plot) at locations P1 (a,b), P2 (c,d) and S1 (e,f). The dotted curves are obtained by neglecting the rotation when solving the stability equations.

8
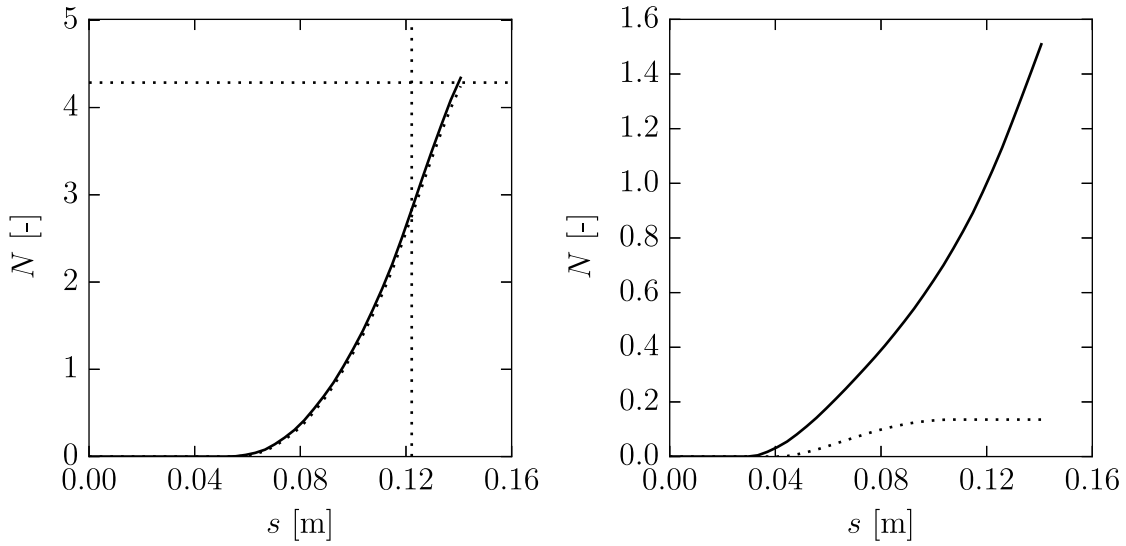
Fig. 7 *N*-factor against the curvilinear abscissa *s* along the line **P1** for Tollmien-Schlichting (left) and stationary cross-flow (right) waves. **Results obtained without rotation terms in the stability equations are plotted with dashed lines. The horizontal dotted line corresponds to the transitional *N*-factor given by the Mack's law while the vertical vertical line depicts the location where transition is detected in elsA.**
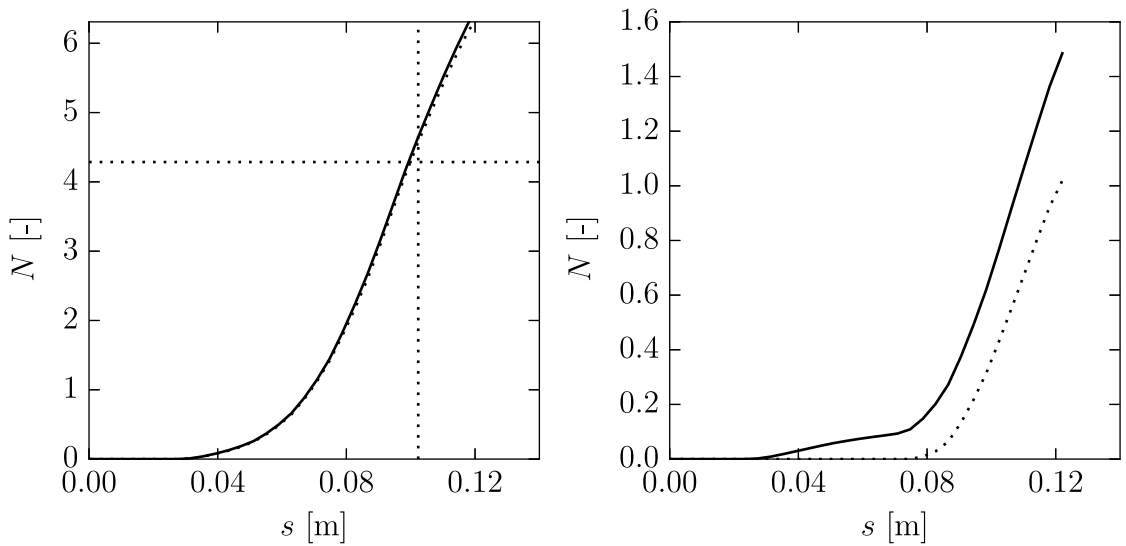
Fig. 8 *N*-factor against the curvilinear abscissa *s* along the line **P2** for Tollmien-Schlichting (left) and stationary cross-flow (right) waves. See the legend figure 7.
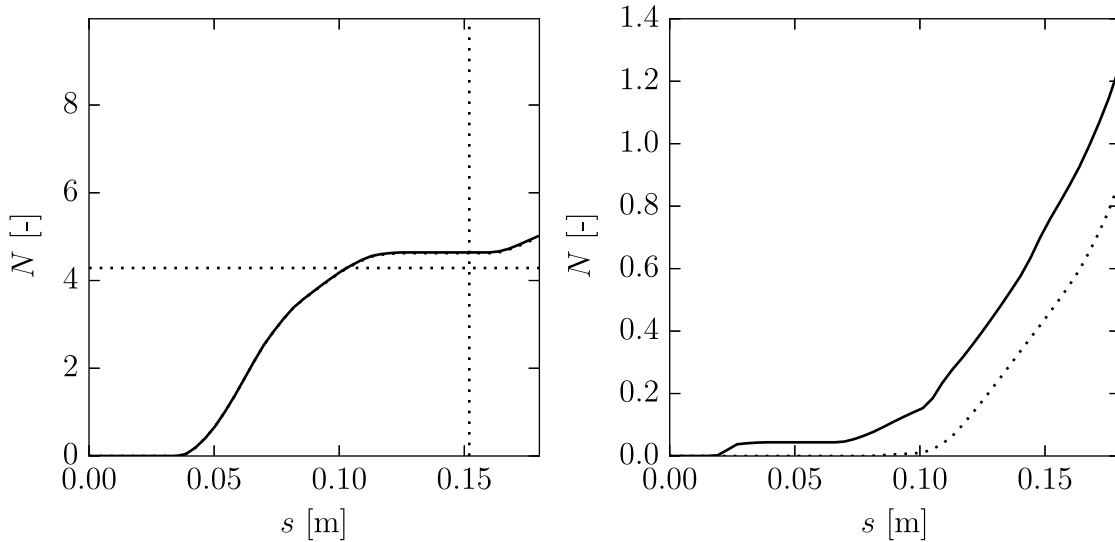
Fig. 9 *N*-**factor against the curvilinear abscissa** *s* **along the line S1 for Tollmien-Schlichting (left) and stationary cross-flow (right) waves. See the legend figure 7.**

too far downstream which can be explained by the fact that the shape of the *N*-factor envelope (almost constant for $s \in [0.11, 0.16]$ m) is quite "pathological".

V. Conclusion

The in-house local linear stability solver of ONERA has been extended to rotating frame by implementing terms corresponding to centrifugal and Coriolis accelerations. Validation was made for the well-known Ekman layer configuration. Moreover, two new validation cases are proposed to validate the implementation of compressible terms. This was motivated by the fact that "only very few test cases combine rotation with compressibility in the litterature" as stated by Dechamps and Hein [11].

The stability solver has been subsequently applied to investigate the effect of rotation on the transition mechanisms of the flow over a fan blade. This was achieved by comparing a set of stability computations accounting for rotation with a set of computations where rotation terms are neglected. Tollmien-Schlichting are found to be hardly modified by rotation while cross-flow waves are destabilised. These findings are in agreement with the work of Dechamps and Hein [11]. The *N*-factors reached by cross-flow waves are seen to be too low to trigger transition which is rather due to the amplification of Tollmien-Schlichting waves. It can be concluded that, when performing RANS computation over a fan blade, accounting for transition by means of longitudinal transition criteria originally derived in stationary frame is justified.

Acknowledgments

References

[1] Arnal, D., "Boundary layer transition: predictions based on linear theory," *In AGARD, Special Course on Progress in Transition Modelling 63 p (SEE N94-33884 10-34)*, Vol. 1, 1994.

[2] Mc Croskey, W. J., "Measurements of boundary layer transition, separation and streamline direction on rotating blades," Tech. Rep. TN D-6321, NASA, 1971.

[3] Schülein, E., Rosemann, H., and Schaber, S., "Transition detection and skin friction measurements on rotating propeller blades," *28th AIAA aerodynamic measurement technology, ground testing and flight testing conference*, Vol. 3202, 2012.

[4] Lang, W., Gardner, A. D., Mariappan, S., Klein, C., and Raffel, M., "Boundary-layer transition on a rotor blade measured by temperature-sensitive paint, thermal imaging and image derotation," *Experiments in Fluids*, Vol. 56, No. 6, 2015, pp. 1–14.

[5] Malik, M. R., Wilkinson, S. P., and Orszag, S. A., "Instability and transition in rotating disk flow," *AIAA Journal*, Vol. 19, No. 9, 1981, pp. 1131–1138.

[6] Garrett, S. J., Hussain, Z., and Stephen, S. O., "The cross-flow instability of the boundary layer on a rotating cone," *Journal of Fluid Mechanics*, Vol. 622, 2009, pp. 209–232.

[7] Potter, M. C., and Chawla, M. D., "Stability of boundary layer flow subject to rotation," *The Physics of Fluids*, Vol. 14, No. 11, 1971, pp. 2278–2281.

[8] Gross, A., Fasel, H. F., Friederich, T., and Kloker, M. J., "Numerical investigation of S822 wind turbine airfoil," *Proceedings of 40th fluid dynamics conference and exhibit. Chicag (USA)*, 2010.

[9] Heister, C., "Semi-empirical transition prediction and application to an isolated rotor in hover," *International Journal of Engineering Systems Modelling and Simulation*, Vol. 4, No. 1–2, 2012, p. 69–78.

[10] Brazier, J.-P., "MAMOUT : Modules d'Analyse MOdale Unidimensionnelle avec les polynômes de Tchebychev. Instructions pour l'emploi des programmes Spectre et Moditer Version 6." Tech. Rep. RT 1/24067 DMAE, ONERA, 2015.

[11] Dechamps, X., and Hein, S., "Extension of the PSE code NOLOT for transition analysis in rotating reference frames," *New Results in Numerical and Experimental Fluid Mechanics XI: Contributions to the 20th STAB/DGLR Symposium Braunschweig, Germany, 2016*, Vol. 136, Springer, Braunschweig, Germany, 2017, p. 179.

[12] Mack, L. M., "Transition prediction and linear stability theory," *In AGARD Laminar-Turbulent Transition 22 p (SEE N78-14316 05-34)*, Vol. 1, 1977.

[13] S. Leibovich, S. K. L., "The influence of the horizontal component of Earth's angular velocity on the instability of the Ekman layer," *Journal of Fluid Mechanics*, Vol. 150, 1984, p. 41–87.

[14] Allen, L., and Bridges, T. J., "Hydrodynamic stability of the Ekman boundary layer including interaction with a compliant surface: a numerical framework," *European Journal of Mechanics-B/Fluids*, Vol. 22, No. 3, 2003, p. 239–258.

[15] Cambier, L., and Gazaix, M., "elsA - An efficient object-oriented solution to CFD complexity," *40th AIAA Aerospace Sciences Meeting & Exhibit*, 2002. 2002-0108.

[16] Arnal, D., Casalis, G., and Houdeville, R., "Practical transition prediction methods: subsonic and transonic flows," *VKI Lectures Series Advances in Laminar-Turbulent Transition Modelling*, 2008.